Broadband Fan Noise Prediction Using Single-Airfoil Theory

Michel Roger[a], Stephane Moreau[b] and Alain Guedel[c]

(Received 2005 March 24; revised 2005 December 09; accepted 2006 January 16)

The present study is dedicated to the analytical modeling of the broadband noise radiated by subsonic fans, such as encountered in HVAC or automotive engine cooling applications. A fan noise prediction scheme is proposed on the basis of single-airfoil linearized unsteady aerodynamics theories. Two basic spanwise distributed mechanisms are considered, namely the noise from the impingement of upstream turbulence, and the trailing edge noise associated with turbulence boundary layer scattering. The associated analytical models are validated by comparing the theoretical results with experimental data collected in open-jet anechoic wind tunnels, and existing numerical computations found in the literature. Validations involve single-frequency directivity, single-direction spectra and radiation maps in a large range of flow conditions over different mock-ups in the midspan plane. The transfer function between the wall-pressure statistics and the far-field sound should be invariant according to the analytical model and is experimentally found to be within ±5 dB with respect to flow conditions encountered on an isolated airfoil. Finally, a first application of the model to a highly twisted, tapered and swept automotive engine cooling fan is presented. In view of the results, trailing-edge noise is found to be significant contributor, at least in the high frequency range beyond 4 kHz for a chord-based Reynolds number of about 2 x 10^5 and Mach number of about 0.1. © ***Institute of Noise Control Engineering***

Primary subject classification: 11.4; Secondary subject classification: 21.6

1 INTRODUCTION

Broadband noise is a major part of the noise radiated by most fans, besides the discrete frequency radiation at the blade passing frequency and harmonics. Random in nature, it is attributed to the turbulence in the flow, and more precisely for the moderate Mach numbers encountered in HVAC applications, to the fluctuating loads induced by the turbulence on moving blades or stationary solid surfaces (inlet guide vanes, stator vanes, casing, flaps, etc.). This interpretation is justified by the acoustic analogy[1]. Different mechanisms are recognized to contribute significantly, which are hard to separate in practice due to their wide spectral extent and the change in relative levels depending on the fan operating point:

1. interaction of blades or vanes with inflow turbulence, either from inlet or casing boundary layers or upstream wakes;
2. trailing-edge noise due to turbulent boundary layers or flow separation on blades or vanes;
3. vortex shedding noise associated with von Kármán vortex streets and related flows;
4. noise generation by leakage flows and tip vortices.

The present paper focuses on the first two, which correspond to sources distributed along the blade span with conditions of attached mean flow at the trailing edge and boundary layer thickness larger than the trailing edge thickness. All mechanisms are just examples of the same basic physical process: some part of the kinetic energy of a vortical flow escapes as sound as soon as the inertia of the vortical motion is suddenly modified by interaction with a singular point on a solid surface. The generic element of the analysis is the isolated airfoil with constant cross-section in a parallel flow, any blade segment in a fan being understood locally as such an equivalent airfoil. The question whether or not the broadband noise from rotating blades can be inferred from a single-airfoil analysis might draw controversy. The first reason is acoustical: the single-airfoil theory takes no account of the mutual scattering of adjacent blades. Existing cascade response functions accounting for this interaction can only be used properly in the context of ducted fans[2]. As a consequence, even though it might be important for fans with sufficient ratio of blade chord length to blade pitch (high solidity), this acoustic rotor effect will be ignored here. The second point is that the flow on a rotating blade may be very different from the one on a single airfoil, because of the periodicity imposed by the solidity and the effects of inertia (radial equilibrium, centrifugation, swirl effect, three-dimensional boundary layers, secondary flows). This can be called the aerodynamical rotor effect. The present approach is not devoted to reproducing the the real flow field in a fan but rather to find out some transfer function between the main statistical features in the flow and the statistics of the corresponding sound field. According to the acoustic analogy, this transfer function itself will be shown to hold for any tested configuration with attached mean flow at the trailing edge. When determined in the simple case of the single airfoil, it can be extended or applied to a fan as explained below. Of course, the specific flow features corresponding to the investigated rotating blades must be known independently, since they only enter the model as source terms. Except in some circumstances when highly elongated turbulent eddies are chopped by a rotor inducing quasi coherent excitation (this happens with the atmospheric turbulence which enters turbofan engines operating on the ground, for instance), turbulence induces source on rotating blades which, actually, are not blade-to-blade correlated. This is met whenever the time it

[a] *Ecole Centrale de Lyon, LMFA, UMR CNRS 5509, 69143, Ecully FRANCE. email: michel.roger@ec-lyon.fr.*
[b] *Valeo Motors and Actuators, 78321 La Verriere FRANCE. email: stephane.moreau@valeo.com*
[c] *CETIAT, 69100 Villeurbanne FRANCE. email: alain.guedel@cetiat.fr*

takes a turbulent eddy to cross the rotor at the axial speed U_z remains smaller than the blade passing period $2\pi/(B\Omega)$, where B is the number of blades and Ω the angular velocity. This condition reads $\Lambda_z << U_z/(B\Omega)$, with Λ_z a streamwise integral turbulence scale. This generally corresponds to a true broadband signature with no peak frequency. The zero blade-to-blade correlation assumption is made here, meaning that the aerodynamics on one blade is not affected by what happens on another one. The consequence is that the total fan noise intensity is simply the sum of the contributions radiated from all blades.

2 ANALYTICAL MODELS

The noise radiated by turbulence interacting with a solid surface is understood as a stationary random process and, as such, must be related to some statistical parameters in the turbulent field. The acoustic analogy[1] states that the equivalent noise sources are the pressure fluctuations induced on the airfoil surface. In the case of the interactions with upstream turbulence, they result from the breakdown of oncoming vortices through the rigid-wall condition at the airfoil surface and the pressure fluctuations concentrated at the leading edge. In the case of trailing edge noise, they result from the Kutta condition and focus at the trailing edge. Within the framework of analytical modeling, this makes the best dedicated mathematical approach different in each case because the physical background is different.

2.1 Turbulence-Interaction Noise

Turbulence-interaction noise can be inferred from linearised theories of unsteady aerodynamics inherited from the pioneering work of van Kármán & Sears[3]. The power spectral density (PSD) of the far-field sound pressure $S_{pp}(\vec{x},\omega)$ is related to the statistics of the upstream turbulent velocity field via spectral turbulent models used as input data. The formulation proposed by Amiet[4] is retained in this paper for its simplicity, its physical consistency and the same mathematical foundations that will be referred to for the trailing-edge noise model described later on. The basic formula is:

$$S_{pp}(\vec{x},\omega)=\left(\frac{\rho_0 kcx_3}{2S_0^2}\right)^2 \pi U_0 \frac{d}{2}\int_{-\infty}^{\infty}\Phi_{ww}\left(\frac{\omega}{U_0},k_2\right)\left|\Im\left(x_1,\frac{\omega}{U_0},k_2\right)\right|^2 \frac{\sin^2\left[\left(\frac{kx_2}{S_0}-k_2\right)\frac{d}{2}\right]}{\pi\frac{d}{2}\left(\frac{kx_2}{S_0}-k_2\right)^2}dk_2 \tag{1}$$

and a simplified expression is obtained when assimilating the result to the asymptotic value for large aspect ratio $d/c\rightarrow\infty$:

$$S_{pp}(\vec{x},\omega)=\left(\frac{\rho_0 kcx_3}{2S_0^2}\right)^2 \pi U_0 \frac{d}{2}\Phi_{ww}\left(\frac{\omega}{U_0},\frac{kx_2}{S_0}\right)\left|\Im\left(x_1,\frac{\omega}{U_0},\frac{kx_2}{S_0}\right)\right|^2 \tag{2}$$

In these expressions, $\vec{x}=(x_1,x_2,x_3)$ stands for the coordinates normal to the airfoil plane and along the airfoil chord and span, respectively. The origin of this reference frame can be chosen at any location along the chord because Eqn. (2) is valid in the geometrical far field. ρ_0 is the fluid mean density, c is the chord length and d the spanwise extent. $k=\omega/c_0$ is the acoustic wavenumber and U_0 the incoming flow velocity. k_2 stands for the aerodynamic wavenumber in the spanwise direction, S_0 is a corrected distance accounting for the sound convection by the surrounding flow[4]. $\Im$ is an aeroacoustic transfer function accounting for the airfoil response. The input data is the two-dimensional spectrum Φ_{ww} of the turbulent velocity component normal to the airfoil chord. The minimum relevant data when more precise information is missing is provided by assuming a homogeneous and isotropic turbulence, described by analytical models such as Liepmann's or van Kármán's. This reduces the statistical inputs to two parameters, the root mean square value of the velocity fluctuations and the integral length scale. The result in the mid-span plane can also be expressed in terms of the velocity PSD $S_{ww}(\omega)$ and the related spanwise correlation length $l_y(\omega)$ which is more easily connected to possible measurements:

$$S_{pp}(\vec{x},\omega)=\left(\frac{\rho_0 U_0 kcx_3}{2S_0^2}\right)^2 \frac{d}{2}\left|\Im\left(x_1,\frac{\omega}{U_0},0\right)\right|^2 S_{ww}(\omega)l_y(\omega) \tag{3}$$

Expressions for Φ_{ww}, S_{ww} and l_y can be found in standard literature on turbulent flows[5,6] or can be obtained either experimentally by hot wire or laser Doppler anemometry, or by detailed Computational Fluid Dynamics, such as Large Eddy Simulations (LES) or Direct Numerical Simulations (DNS). A possible alternative to those direct but expensive numerical methods could be the two-step procedure proposed by Lysak and Brungart[7] that combines cheaper Reynolds-Averaged Navier-Stokes (RANS) simulations with an assumption of local turbulence isotropy at each grid node. The local calculated values of the turbulence variable are used to re-compute the von Kármán constants, such as the root-mean-square velocity or the longitudinal integral length scale, on the CFD grid.

The most important factor in Eqns. (1) to (3) is the aeroacoustic transfer function $\Im$ that determines the radiation efficiency of the incoming disturbances. The wall pressure field does not enter the formulation directly though it is the true source of the sound. The airfoil acts as a convecter of velocity fluctuations into pressure fluctuations. Expressions for $\Im$ have been given by Paterson and Amiet[8]. They are reproduced in the Appendix.

2.2 Trailing-Edge Noise

Again the model presented here was first proposed by Amiet[9], using the same mathematical approach. The incident turbulence in the boundary layer convected past the trailing edge is accounted for through its pressure trace on the wall. This trace is distorted by the Kutta condition, inducing secondary pressure fluctuations that act as the equivalent sound sources. This is why the fluctuating pressure is used as the aerodynamic variable instead of the fluctuating velocity. The final expression of the far-field sound for a large aspect ratio is similar to the one for turbulence-interaction noise according

to Eqn. (3):

$$S_{pp}(\vec{x},\omega)=\left(\frac{kcx_3}{2\pi S_0^2}\right)^2\frac{d}{2}\left|\Im'\left(x_1,\frac{\omega}{U_0},0\right)\right|^2\Phi_{pp}(\omega)l_y\left(\frac{\omega}{U_c}\right) \quad (4)$$

except that the input data refer to the pressure statistics. Φ_{pp} is the aerodynamic wall-pressure spectrum that is induced close to the trailing edge only by the incident turbulence (ignoring the contamination by the Kutta condition). U_c is the local convection speed of the boundary layer disturbances. $\Im'$ is another aeroacoustic transfer function which now depends on U_c. An expression for $\Im'$ was initially proposed by Amiet. Some extensions have been added by Roger and Moreau[10] to account for leading-edge back-scattering and three-dimensional pressure patterns. These are also reproduced in the Appendix. The key point now is to get the needed information on Φ_{pp}, l_y, and U_c from the wall-pressure field. Very different flow conditions may be encountered in practice, corresponding to different wall-pressure statistics: attached turbulent boundary layers with adverse pressure gradients, separated flows, and so on. Previously published model data for boundary layers over flat plates[11], which play the same role as the Liepmann's and von Kármán's models for velocity statistics, cannot cover the whole range of real flows. The practical use of Eqn. (4) will be discussed together with the validations presented later on in the paper. It is limited to boundary layer flows for which a streamwise convection speed can be deduced from the wall pressure statistics. This a priori excludes separated flows with a recirculation bubble at the trailing edge.

Sample results for the radiation efficiency, defined as $|kcx_3/S_0|$ times the modulus of the aeroacoustic transfer function $\Im$ or $\Im'$ are given in Fig. 1 for a Mach number of 0.05. They are an illustration of the directivity patterns in the mid-span plane. Trailing-edge noise sources radiate preferentially upstream and turbulence-interaction noise sources preferentially downstream, as the reduced frequency *kc* increases. The number of lobes is determined primarily by *kc* and less importantly by the Mach number.

Some confusions must be avoided here. In actual complex fan system configurations, both noise mechanisms co-exist and cannot be easily separated in the far field measurements. However, in single airfoil experiments with impinging turbulence intensity below 1 %, source localization techniques can be applied at high frequencies to demonstrate that the trailing edge noise is dominant (see for instance, Brooks et al[12,13,14] or Oerlemans and Migliore[15,16]). The present study does not intend to discriminate between the different noise sources, but rather to provide an analytical diagnosis tool to be tested against measurements[17]. Moreover, it is assumed that the turbulence scales remain small enough according to Amiet's high frequency formulation, so that both mechanisms can be dealt with separately in a linear analysis. Nevertheless, the scattering of incident turbulence at an airfoil or blade leading edge involves a trailing edge contribution (associated with the Kutta condition). In the same way, the scattering of boundary layer turbulence at the trailing edge involves a leading edge correction.

2.3 Application to Rotating Blades

Locally, the flow features on a rotating segment are not fundamentally different from what happens on an isolated airfoil, except for the aerodynamic three dimensional effects due to inertial acceleration and radial pressure gradients. Therefore the transfer functions from single-airfoil theories can be applied to predict the noise radiated to the far field by a complete fan, provided that the required information is available at different radii and that the flow remains attached on the blade. The main idea is that the circular motion can be considered locally as tangent to an equivalent translating motion, for which the aforementioned formulae hold. This is true only for sound frequencies higher than the rotational frequency. Initially developed for high-speed blades of model helicopter rotors in wind-tunnel testing[18], the analysis presented here is specified to low Mach number fans operating in a medium at rest.

Let $\vec{x} = (x_1, x_2, x_3)$ now be the instantaneous coordinates of the observer in a reference frame attached to a blade segment at angle Ψ (Fig. 2). At the corresponding instant the surrounding fluid is moving with respect to the blade with the velocity U induced by rotation and assumed parallel to the chord line in accordance with the weakly loaded airfoil assumption in the linearised theory. Sound propagates towards the observer according to the convected Helmholtz equation expressed in the reference frame (x_1, x_2, x_3) and the solution would be exactly given by the single-airfoil formulae, were the translating motion frozen. Since the blade is moving with respect to the observer, the instantaneous emitted frequency $\omega_e(\Psi)$ at the current position $\Psi = \Omega t$ and corresponding to the given frequency received by the observer ω is determined by the Doppler factor, according to the equation:

$$\frac{\omega_e(\Psi)}{\omega}=1+M\sin\Theta\sin\Psi=1-M_r \quad (5)$$

where $M = \Omega R_0 / c_0$ is the rotational Mach number at radius R_0 for angular velocity Ω and M_r denotes the relative Mach number, projection of M in observer's direction. The sound heard at frequency ω is produced by sources on the rotating blade segment having different frequencies depending on their angular position. The resulting spectrum must be calculated by averaging over all possible angular locations of the blade segment and weighting by the Doppler ratio. This is made according to the equation:

$$S_{pp}(\vec{x},\omega)=\frac{B}{2\pi}\int_0^{2\pi}\frac{\omega_e(\Psi)}{\omega}S_{pp}^{\Psi}(\vec{x},\omega_e)\,d\Psi \quad (6)$$

in which $S_{pp}^{\Psi}(\vec{x}, \omega_e)$ denotes the noise spectrum that would be radiated from the current blade segment at angle Ψ ignoring the Doppler frequency shift. $S_{pp}^{\Psi}(\vec{x}, \omega_e)$ is precisely what is provided by the single-airfoil formulae. When applying Eqn. (6), the change of system of coordinates must be performed according to the sketch of Fig. 2. The low Mach number

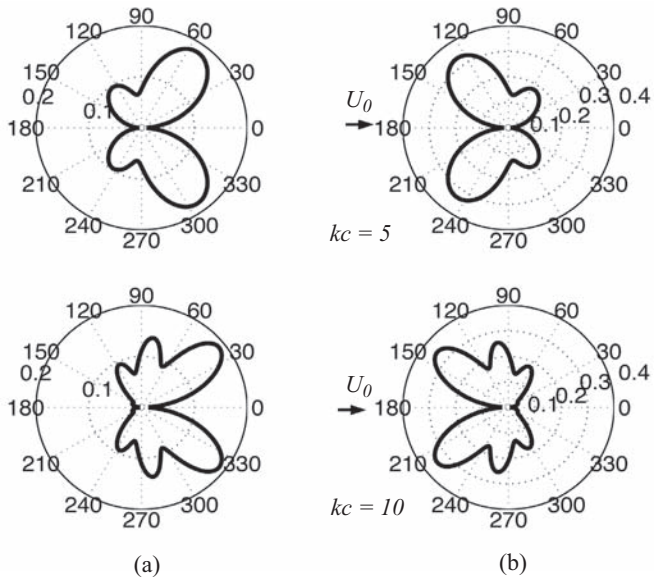

Fig. 1. Typical directivity patterns of (a): turbulence-interaction noise, and (b); trailing-edge noise, according to the analytical models. M_0=0.05 and Ψ=90° (midspan plane).

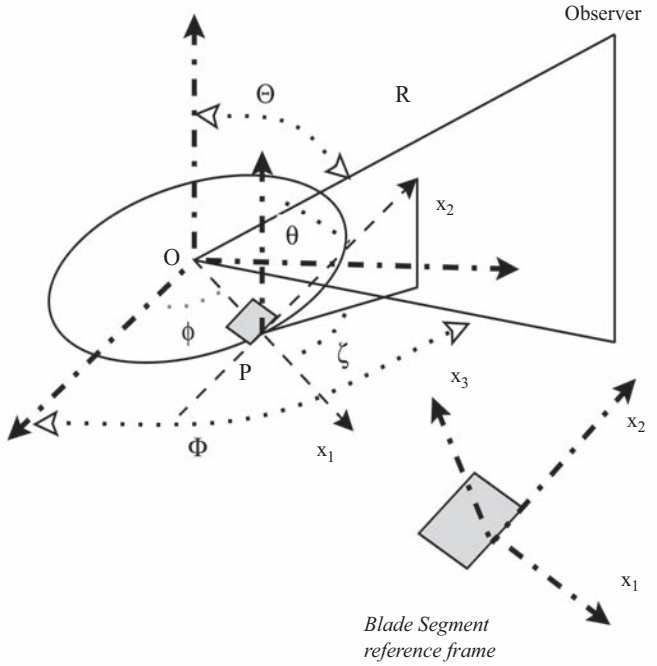

Fig. 2. Fan reference frames with a blade segment at point P (trailing-edge noise configuration). Observer's coordinates (R,Θ,Φ) with respect to rotor frame: trailing-edge line along x_2-axis. (θ,ς) are the orientation angles of the trailing-edge line with respect to rotor axes (ς=0 and θ=π/2 for axial non-swept blades).

applications and broadband noise with flat and wide frequency content, the Doppler frequency shift has no significant effect. Yet, it is kept in the calculations for the sake of physical consistency (energy conservation and spectral spreading in the definition of a PSD).

3 EXPERIMENTAL SET-UP FOR VALIDATION

The key point of the theoretical models is the transfer function $\mathfrak{I}$ or $\mathfrak{I}'$ that can be defined between the wall-pressure statistics or the oncoming velocity statistics and the far field sound. The following sections are devoted to the experimental validation. The transfer function must be shown to be independent of the flow parameters as long as the same generating mechanism is involved. This is achieved here for trailing-edge noise only. More precisely, attached turbulent boundary layers, laminar unstable boundary layers and nearly-separated boundary layers must obey the same transfer function, the difference being only in the wall-pressure statistics entering the model as input data. Equivalent validation cases for the leading edge noise can be found in Refs. [17 and 19].

The experimental set-up, shown in Fig. 3, is installed in an open-jet anechoic wind tunnel. The airfoil is held between horizontal side-plates fixed to the nozzle. Two rotating disks inside the plates allow adjusting the angle with respect to the flow. The operating point of the investigated airfoil is set by varying the angle of attack. Sound is measured in the far field in the mid-span plane using a standard B&K 1/2-inch microphone on a moving arm. The wall-pressure fluctuations are measured at the same time using a set of flush-mounted Remote-Microphone Probes (RMP), so that the transfer function and other statistical quantities required in the analytical formulation (convection speed) can be deduced. The same procedure can be repeated with the same installation on different airfoils. Measurements have been performed on a reference NACA 0012 airfoil (10 cm chord length), a thin cambered Control-Diffusion airfoil (13.6 cm chord length and 4% relative thickness) designed by VALEO and a flat plate (10 cm chord length and 3% relative thickness). The aim is to check the validity of the analytical prediction scheme with different cambers and/or thickness.

3.1 Installation Effects

Experimental investigations of airfoil self noise made in wind tunnel facilities draw us to address the question of spurious effects due to the installation. Some of these effects are purely aerodynamical, as pointed out by Moreau et al[20]: a lifting airfoil in an open jet of limited extent is responsible for a flow deflection due to the momentum injection. As a result, the pressure coefficient distribution over the airfoil surface is different from what would be found in free air. This point is not addressed here, the goal being the validation of a transfer function which does not depend on the flow conditions. The second effect is acoustical: the sound field radiated by the airfoil is distorted due to scattering by the nozzle lips or other solid surfaces of the set-up. This is essentially true in anechoic open jet wind tunnels: the airfoil is held between

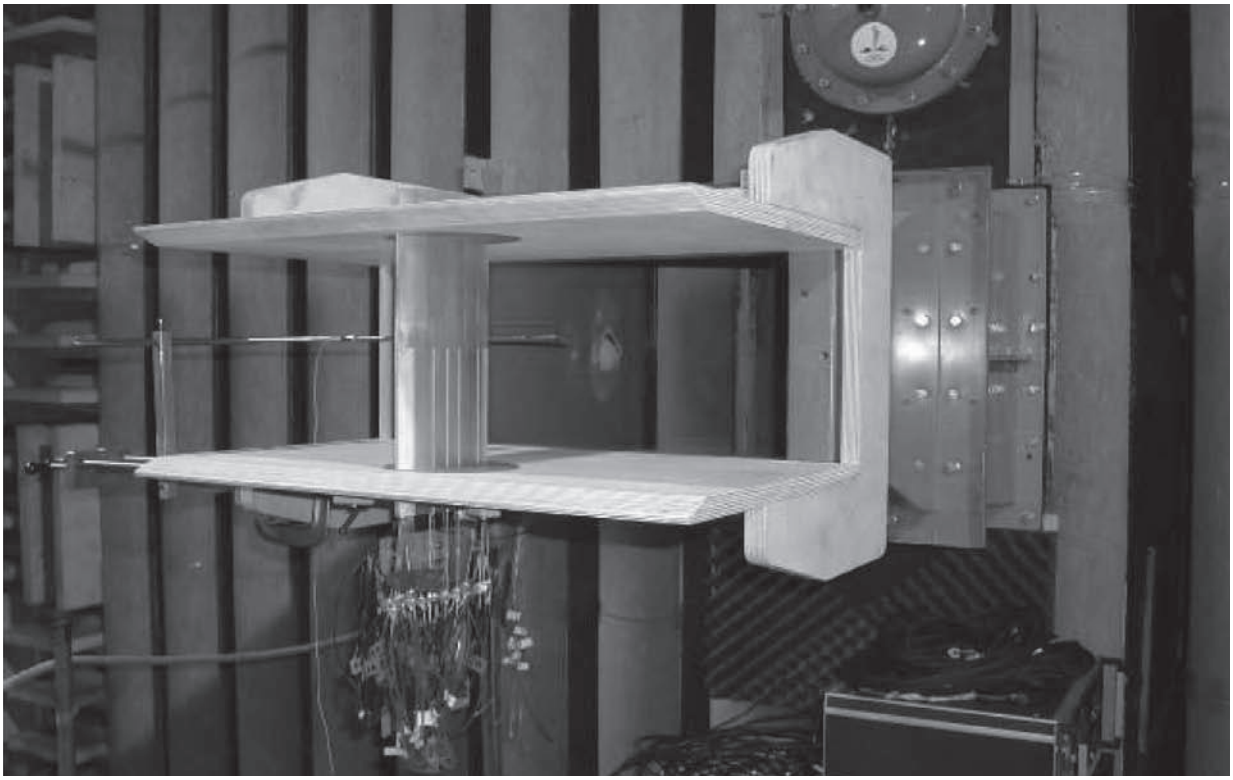

Fig. 3. Experimental set-up at ECL, featuring the nozzle geometry and the VALEO CD airfoil with Remote Microphone Probes.

two side-plates quite close to the nozzle lips, such that it is embedded in the potential core of the jet. Part of the sound radiated in the forward direction and normally not measurable is diffracted at the lips and the diffracted field contaminates the direct field to be compared with the theoretical results. This is crucial for self-noise at higher frequencies, for which sound focuses upstream, as well as a lower frequencies because of the proximity of the nozzle in terms of acoustic wavelengths. Since any measurement combines both the direct and scattered fields, the installation effect cannot be corrected by post-processing the measurements and must be rather included in the theoretical simulation. In principle, it cannot be ignored in the validation procedure. For the sake of simplicity, the nozzle scattering is only accounted for in the validation at single frequencies described below. It will be omitted in the subsequent broadband applications.

3.2 Single-Frequency Directivity Assessment

The directivity is defined here by the radiation efficiency $|kc\Im' x_3 / S_0|$ plotted as a function of θ, the angle in the midspan plane from the chord line (Fig. 1). The best way to validate this variable, irrespective of the flow conditions, is to generate trailing-edge noise sources with tonal excitation. This has been done here with a NACA 0012 airfoil at zero angle of attack. In that configuration, the boundary layers are laminar and unstable in the aft part of the airfoil, leading to the onset of Tollmien-Schlichting (TS) waves. Due to acoustic back-reaction[21], self-sustained oscillations occur at discrete frequencies selected by the feed-back loop parameters and strong tones are heard in the far field. An isolated tone is associated with wall-pressure fluctuations that are almost perfectly spanwise correlated being triggered by the acoustic waves generated at the trailing edge[22]. For that reason, the isolated TS radiation is a nearly two-dimensional process with respect to an observer in the distant mid-span plane and, as such, is the exact experimental illustration of the basic analytical solution as given in Eqn. (4). Therefore measured and computed directivity patterns should agree at best. The directivity measurements over the angular range covered in the experiment at a reduced frequency of about 5 exhibit a three-lobed pattern, as shown in relative decibels in Fig. 4, whereas the analytical free-field solution (ignoring the nozzle effect) is strongly different. The levels have been adjusted using an arbitrary constant since only the directivity is addressed here. Then the nozzle scattering has been numerically computed in a 2D configuration using the SYSNOISE software, and applied to the analytical simulation. The final theoretical results, also plotted in Fig. 4, agree very well with the measurements. This definitely validates the analytical model.

Apart from the experimental validation, the present analytical solution compares very well with Howe's calculations based

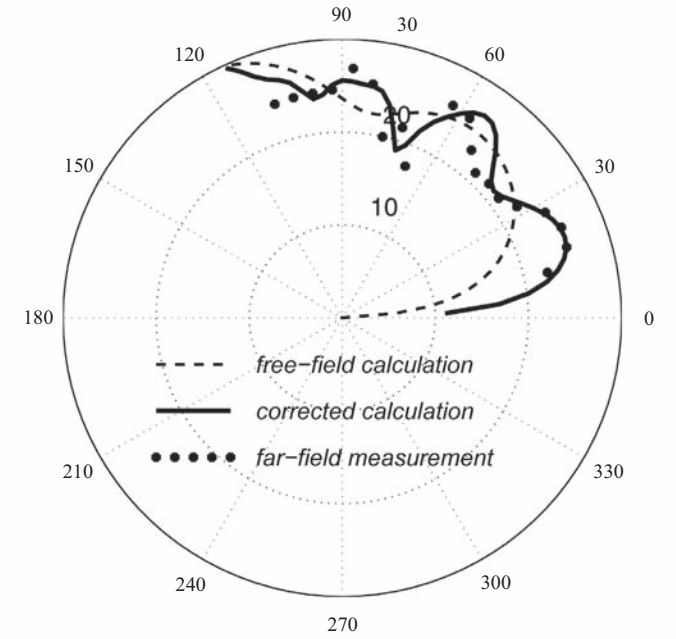

Fig. 4. Measured directivity of a TS tone compared with theoretical results assuming free-field and correction for nozzle scattering, dB-scale; kc=4.88.

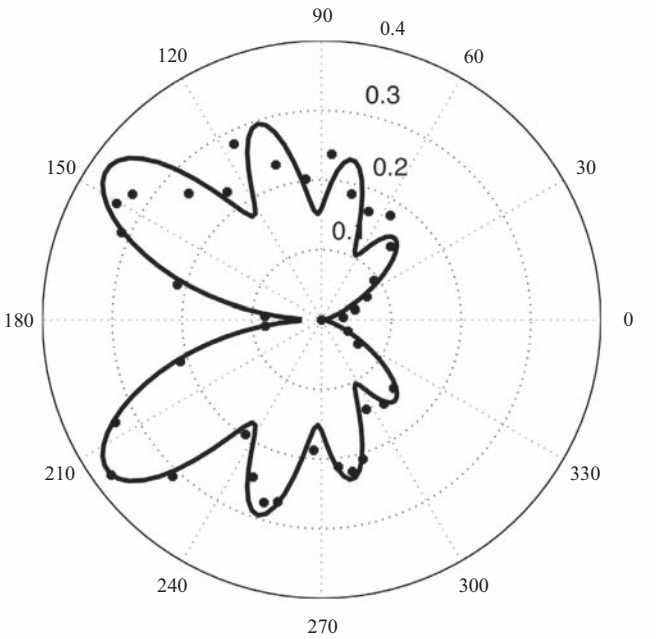

Fig. 5. Free-field analytical directivity pattern (solid lines) compared with numerical results (symbols) of Ref. [24] for a cambered airfoil; kc=4π.

on a multiple-scattering Green's function[22,23]. Furthermore, the single-frequency, analytical transfer function for the flat plate can be compared to numerical simulations to assess the importance of some ignored parameters, such as camber and thickness. A typical result is given in Fig. 5, where the directivity of the analytical radiation efficiency is compared to a two-dimensional computation of the Green's function of a slightly cambered airfoil for sources close to the trailing edge[24]. The flat-plate assumption made in the model does not allow for the reproduction of the slight differences between sounds radiated from the pressure and suction sides, but the errors remain small enough in terms of decibels to make the analytical solution useful for application to any airfoil shape with moderate thickness and camber.

3.3 Spectral Validations

The analytical model of trailing-edge noise has been tested against previously published experimental results. The theoretical noise spectra given by Eqn. (4) are first compared with some measurements by Schlinker and Amiet[25] in Fig. 6. Schlinker and Amiet did not measure the wall-pressure statistics and used NACA-0012 measurements from Yu and Joshi[26] instead. The same is done here. The comparison with the results of Brooks and Hodgson[12] is shown in Fig. 7. The corresponding measured wall pressure spectra and mean convection speed ($U_c = 0.6U_0$), available in that case, were used. A fairly good agreement is obtained in both cases but the predicted noise levels are very sensitive to the input values of the convection speed and the spanwise correlation length. Moreover the measured wall pressure spectra should always be preferred to yield the proper spectral shape and level.

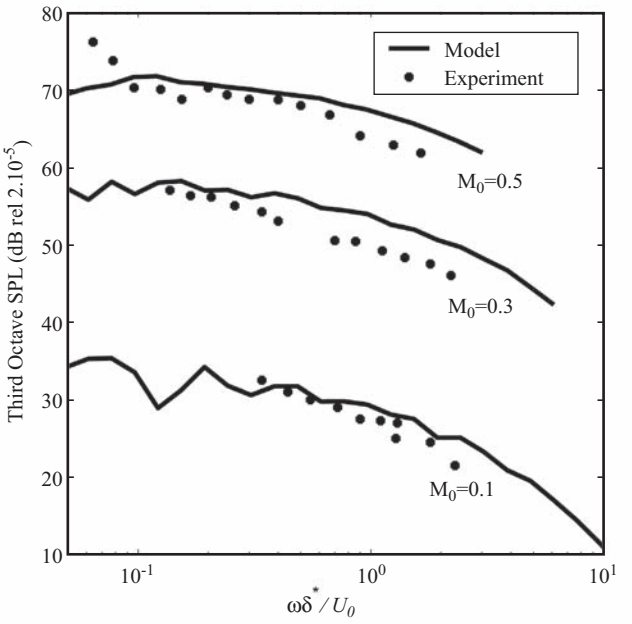

Fig. 6. Analytical trailing-edge noise model against the experimental results of Ref [25]. Helicopter blade profile in the mid-span plane at 70°.

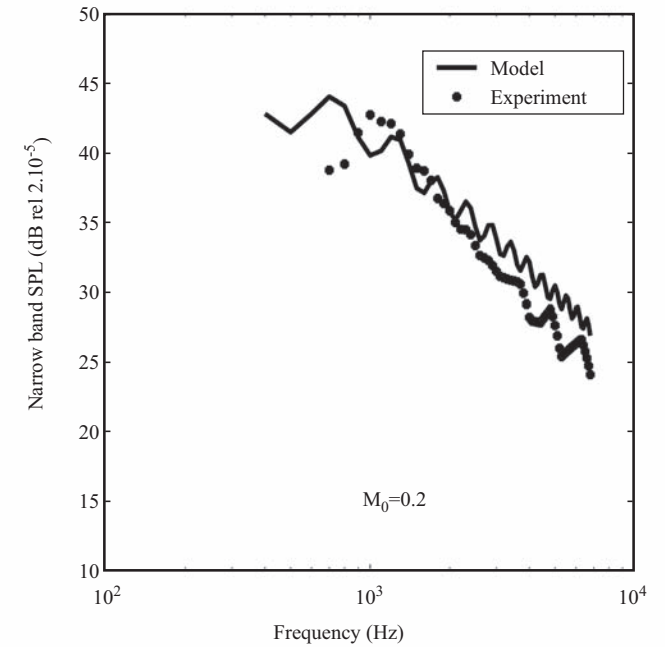

Fig. 7. Analytical trailing-edge noise model against the experimental results of Ref. [12] (Fixed bandwidth 1 Hz). NACA-12 airfoil in the mid-span plane at 90°.

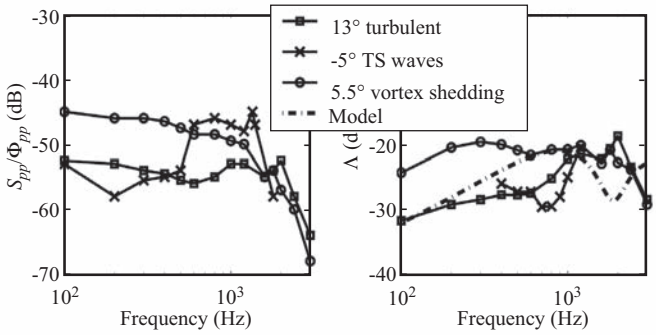

Fig. 8. Experimental evidence of an invariant Λ for trailing-edge noise radiation on the VALEO CD airfoil, from Ref. [22]. Observer in the mid-span plane, at 90° from chord line direction. Dashed-dotted line: free-field analytical solution.

3.4 Transfer Function Invariance

The function $\Im'$ being determined analytically on the basis of purely acoustical arguments, it cannot depend on the flow conditions in principle. This has been checked by performing measurements on the Controlled Diffusion (CD) cambered airfoil with different angles of attack, corresponding to a laminar boundary layer with TS waves, an attached turbulent boundary layer and a nearly separated boundary layer on the suction side. In each case, Φ_{pp} and S_{pp} have been measured with standard techniques and l_y evaluated by means of spanwise coherence measurements. In the case of the TS waves the tones amplified by the feedback loop have been removed since they do not correspond to a true random process and only the narrow-band natural instability spectrum, with a much smaller spanwise correlation length than the tones, has been retained[22]. The ratio S_{pp} / Φ_{pp} is first plotted in Fig. 8-left, showing no universal trend.

The non-dimensional ratio $\Lambda = \left(\frac{S_0^2}{x_3}\right)^2 S_{pp} / \left(\Phi_{pp} l_y d\right)$, proportional to $\Im'$ according to Eqn. (4), has been deduced from the measurements and is plotted in Fig. 8-right. Apart from remaining discrepancies that can be attributed to the difficulty of measuring l_y properly over the whole frequency range of interest, a collapse within a couple of decibels is observed above 1000 Hz. The analytical solution from Eqn. (4) for Λ is also included in the figure (dashed-dotted line). The nozzle scattering is not accounted for here, explaining the apparent disagreement. However the right order of magnitude is achieved.

3.5 Radiation Maps

The following results (Fig. 9(a) & (b)) are presented as radiation maps with radiation angle and frequency as coordinates for the CD airfoil. The background noise as measured when the airfoil is removed has been subtracted. On the one hand, this provides an easy overview of a large amount of data. On the other hand, since the model is expected to reproduce both the directivity and the frequency content, a general agreement is better sought directly on the radiation map than just on a single-frequency directivity pattern or a noise spectrum at a single radiation angle.

The acoustic levels are in decibels. The measured radiation map in Fig. 9(a) exhibits a typical broadband signature. The symmetry of the radiated field with respect to the chord line is almost perfect, as expected from the results of Fig. 5. The calculated radiation map in Fig. 9(b) reproduces the main trends fairly well, except for the fringes due to the nozzle scattering. The sound field is directly calculated using Eqn. (4) and the measured wall-pressure statistics Φ_{pp}, l_y, U_c, without any adjustment. Even though some discrepancies remain, this is considered an encouraging result. The maps also show the more pronounced upstream radiation as frequency increases, typical of trailing-edge sources.

4 ROTATING BLADE VALIDATION

The final issue in the validation is the application of the single-airfoil theory to a fan according to Eqn. (6) and the comparison with broadband noise measurements on a real fan. For that a strip theory is applied and a rotating blade is split into segments of different radii. Values of Φ_{pp}, l_y, U_c, must be provided for every segment. This information is hardly available in practice, only for a very limited number of

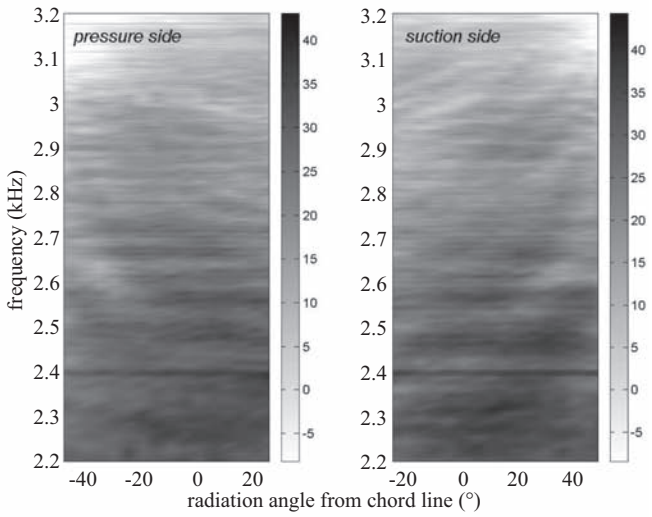

Fig. 9. Radiation maps for the CD airfoil. (a) Experiment and (b) Analytical free-field model. Velocity 16 m/s; 15° angle of attack relative to the mean camber line.

airfoil shapes under specific flow conditions as tested above or computed by more sophisticated methods, such as the Large Eddy Simulation (LES). This is the reason why the search for universal models of the wall-pressure spectrum and/or the spanwise correlation length has received deep attention. The main idea is to the first relate Φ_{pp} to some averaged aerodynamic parameters characteristic of the boundary layer developing on the blade. In Ref. [27] for instance, the wall pressure PSD at the trailing edge was made nondimensional with respect to the external parameters of the local boundary layer, i.e. the displacement thickness close to the trailing edge. This value was obtained either from single hot-wire measurements in the near wake or from RANS computations. For l_y, models are still scarce for various flow conditions. The classical Corcos' model can be referred to in the case of attached turbulent boundary layers and a Gaussian model has been proposed by Roger and Moreau in the case of the nearly separated flow on a loaded airfoil[22].

The implementation of the model has been assessed on the helicopter rotor test case of Schlinker and Amiet[25]. The results, shown in Fig. 10, are similar to those mentioned in the referenced paper, even though the more general formulation for a finite aspect ratio, similar to Eqn. (1), has been used here. On the one hand, the trailing-edge noise model clearly underestimates the measured noise. On the other hand, turbulence-interaction noise, modeled here with a realistic atmospheric turbulence level, certainly dominates. A first attempt has been made with a cooling fan designed by VALEO. The exact forward swept fan configuration has been used to yield the proper emission frequencies and the inlet flow conditions at each strip have been provided by a 3D RANS simulation. In these numerical results, the chord lengths vary from 0.05 to 0.07 m and the relative velocities range from 10 to 30 m/s from hub to tip. The nominal rotational speed of 2500 rpm has also been used. Fig. 11 compares the results using the available experimental Φ_{pp}, l_y, U_c, values at two flow regimes[22,27], namely attached and nearly separated turbulent boundary layers, arbitrarily repeated over the whole span. Both calculations collapse nicely at high frequencies as expected from the wall pressure spectra and match well with the measured narrow bandwidth spectrum for frequencies beyond 4 kHz. The result for highly-loaded blades (solid line) also suggests that some of the medium frequency range

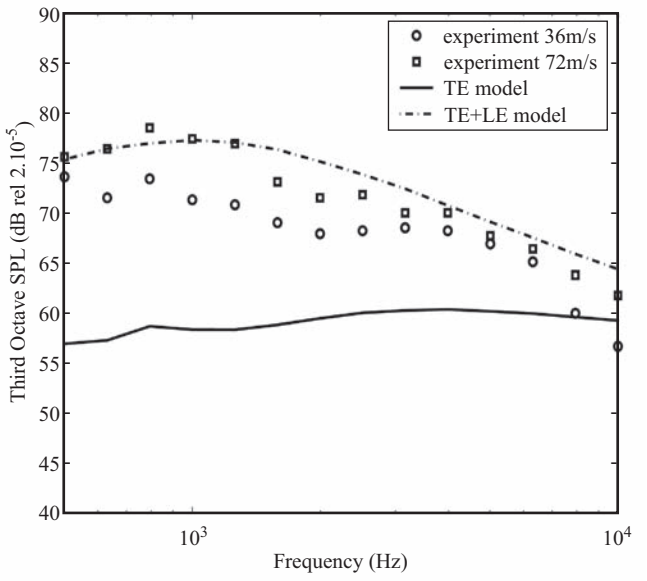

Fig. 10. Application to the helicopter test case of Schlinker and Amiet.

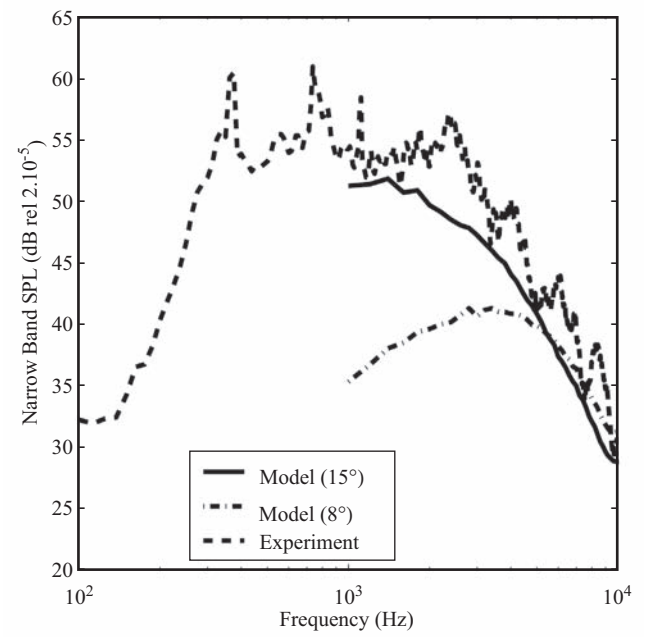

Fig. 11. Automotive engine cooling fan spectra (Fixed bandwidth 2 Hz). Single-airfoil input data at 8° and 15° angles of attack, corresponding to moderate and high loadings

(between 1 and 4 kHz) could be explained by larger angles of attack on the tip sections than expected from inlet speed triangles due to the tip clearance recirculation flow.

5 CONCLUSIONS

Previously published analytical models have been collected and extended in this paper to propose an integrated prediction scheme of the broadband noise radiated by a fan due to spanwise distributed sources. Two mechanisms are accounted for, namely turbulence-interaction noise and trailing-edge noise. The model is dedicated to post-process flow computations made in an industrial context with RANS fast-running codes. The goal is to assess the relative importance of both generating mechanisms with no arbitrary adjustment, instead of using some semi-empirical approach. The models require some statistics of the turbulent flows as input data. Part of these statistics not provided by RANS codes must be replaced by ad-hoc models still under development or by limited experimental data.

A preliminary validation process has been described, essentially for the trailing-edge noise model, equivalent results being available in the existing literature for the turbulence-interaction noise model. The model has been compared to dedicated wind-tunnel experiments involving different airfoil shapes, with moderate camber and thickness. The predicted trailing-edge noise directivity is in very good agreement with the measured one, suggesting that a single-airfoil theory assimilating the airfoil to a flat plate with zero thickness is well suited for fan broadband noise modeling. The model can be applied to any blade segment of a fan, provided that the wall-pressure statistical parameters are known, namely the PSD, spanwise coherence and mean convection speed of the pressure field induced by the oncoming boundary-layer turbulence. The application to a real fan has shown that trailing-edge noise dominates at higher frequencies and may be significant in the middle-frequency range if off-design conditions are achieved. This suggests that the single-airfoil theory provides reliable results for free-field low speed fan with typical solidities between 0.5 and 1.

The present study still needs to be completed by the assessment of the other two generating mechanisms in the introduction, e.g. the vortex-shedding noise and the tip-vortex noise. The aim is to develop physically consistent models for all contributing mechanisms as tools for low-noise design of fans through flow control.

6 APPENDIX

In the mid-span plane $x_2 = 0$, the following expressions hold for the functions $\mathfrak{I}$ and $\mathfrak{I}'$. For off-mid-span plane applications, generalized expressions can be deduced from Graham's similarity rules[28] and equivalent developments. Similarly, only supercritical gusts are considered here. The trailing edge noise expression for the subcritical gusts can be found in Ref. [10]. The following parameters are common to both noise mechanisms:

- Mach number and associated variables:

$$M = \frac{U_0}{c_0} \qquad \beta^2 = 1 - M^2$$

- Streamwise convection wavenumber and associated reduced wavenumbers:

$$K = \frac{\omega}{U_0} \qquad \overline{K} = K\frac{c}{2} \qquad \overline{K}_1 = \frac{\omega c}{2U_c} = \xi\overline{K}$$

$$\overline{\kappa}^2 = \overline{\mu}^2 - \frac{\overline{k}_2^2}{\beta^2} \qquad \overline{\mu} = \frac{\overline{K}M}{\beta^2}$$

$\overline{k}_2$ being the nondimensional hydrodynamic wavenumber in the spanwise direction (zero for the present case).

6.1 Turbulence-Interaction Noise

$$\mathfrak{I} = \mathfrak{I}_1 + \mathfrak{I}_2$$

with the main leading edge contribution (Eqn. (15a) in Ref. [8]):

$$\mathfrak{I}_1\left(x_1, \frac{\omega}{U_0}, 0\right) = \frac{i}{\pi} e^{i\Theta_2} \sqrt{\frac{2}{(1+M)\overline{K}\Theta_1}} E^*\left(2\Theta_1\right)$$

$$\Theta_1 = \overline{\mu}\left(1-\frac{x_1}{S_0}\right) \qquad \Theta_2 = \overline{\mu}\left(M-\frac{x_1}{S_0}\right)-\frac{\pi}{4}$$

and the trailing edge back-scattering correction (Eqn. (15b) in Ref. [8]):

$$\frac{1}{H_2}\Im_2\left(x_2,\frac{\omega}{U_0},0\right) = i\left(1-e^{-2i\Theta_1}\right)+(1-i)\left(E^*(4\overline{\mu})-E^*\left(2\overline{\mu}\left(1+\frac{x_1}{S_0}\right)\right)\sqrt{\frac{2}{1+\frac{x_1}{S_0}}}e^{-2i\Theta_1}\right)$$

with

$$H_2 = \frac{e^{i\Theta_2}}{\pi\Theta_1\sqrt{2\pi(1+M)\overline{K}}}$$

6.2 Trailing-Edge Noise

$$\Im' = \Im'_1 + \Im'_2$$

with the main trailing-edge contributions (Amiet[9])

$$\Im'_1\left(x_1,\frac{\omega}{U_0},0\right) = -\frac{e^{2iC}}{iC}\left\{1+(1+i)e^{-2iC}\sqrt{\frac{B}{B-C}}E^*[2(B-C)]-(1+i)E^*(2B)\right\}$$

$$B = \overline{K}_2 + M\overline{\mu} + \overline{\kappa} \qquad C = \overline{K}_1 - \overline{\mu}\left(\frac{x_1}{S_0}-M\right)$$

and the leading edge back-scattering correction:

$$\frac{1}{H}\Im'_2\left(x_1,\frac{\omega}{U_0},0\right) = \left\{e^{4i\overline{\kappa}}\left[1-(1+i)E^*(4\overline{\kappa})\right]\right\}^{\varepsilon} - e^{2iD} + i\left[D+\overline{K}+(M-1)\overline{\kappa}\right]G$$

with

$$H = \frac{(1+i)e^{-4i\overline{\kappa}}\left(1-\Theta^2\right)}{2\sqrt{\pi}(\alpha-1)\overline{K}\sqrt{B}} \qquad D = C-\left(\overline{K}_1+M\overline{\mu}-\overline{\kappa}\right)$$

$$G = (1+\varepsilon)e^{i(2\overline{\kappa}+D)}\frac{\sin(D-2\overline{\kappa})}{D-2\overline{\kappa}} + (1-\varepsilon)e^{i(-2\overline{\kappa}+D)}\frac{\sin(D+2\overline{\kappa})}{D+2\overline{\kappa}}$$
$$+\frac{(1+\varepsilon)(1-i)}{2(D-2\overline{\kappa})}e^{4i\overline{\kappa}}E^*(4\overline{\kappa}) - \frac{(1-\varepsilon)(1+i)}{2(D+2\overline{\kappa})}e^{-4i\overline{\kappa}}E(4\overline{\kappa})$$
$$+\frac{e^{2iD}}{2}\sqrt{\frac{2\overline{\kappa}}{D}}E^*(2D)\left[\frac{(1+i)(1-\varepsilon)}{D+2\overline{\kappa}} - \frac{(1-i)(1+\varepsilon)}{D-2\overline{\kappa}}\right]$$

and

$$\Theta = \sqrt{\frac{\overline{K}_1+\overline{\mu}M+\overline{\kappa}}{\overline{K}+\overline{\mu}M+\overline{\kappa}}} \qquad \alpha = \frac{U_0}{U_c} \qquad \varepsilon = \left(\sqrt{1+\frac{1}{4\overline{\kappa}}}\right)^{-1}$$

E is a combination of Fresnel integrals and the asterisk denotes its complex conjugate:

$$E^*(x) = \int_0^{\infty}\frac{e^{-it}}{\sqrt{2\pi t}}dt$$

The second term $\Im'_2$ can be ignored for simplicity, except at lower frequencies[22].

7 REFERENCES

1 J.E. Ffowcs Williams and D.L. Hawkings, "Sound generated by turbulence and surfaces in arbitrary motion," Phil. Trans. Roy. Soc., **A264**, 321-342 (1969).

2 S. Glegg, "The response of a swept blade row to a three-dimensional gust," J. Sound Vibr., **227**(1), 29-64 (1999).

3 T. von Kármán and W.R. Sears, "Airfoil theory for non-uniform motion," J. Aero. Sci., **5**, 379-390 (1938).

4 R.K. Amiet, "Acoustic radiation from an airfoil in a turbulent stream," J. Sound Vibr., **41**(4), 407-420 (1975).

5 J.O. Hinze, *Turbulence* (McGraw-Hill, New York NY, (1959).

6 S.B. Pope, *Turbulent Flows* (Cambridge University Press, Cambridge, 1986).

7 P.D. Lysak and T.A. Brungart, "Velocity spectrum model for turbulence ingestion noise from computational-fluid-dynamics calculations," AIAA J., **41**(9), 1827-1829 (2003).

8 R.W. Paterson and R.K. Amiet, "Acoustic radiation and surface pressure characteristics of an airfoil due to incident turbulence," NASA CR-2733 (1976).

9 R.K. Amiet, "High frequency thin-airfoil theory for subsonic flow," AIAA J., **14**(8), 1076-1082 (1976).

10 M. Roger and S. Moreau, "Back-scattering correction and further extensions of Amiet's trailing-edge noise model. Part I: Theory," J. Sound Vibr., **286**(3), 477-506 (2005).

11 W.K. Blake, *Mechanics of Flow-Induced Sound and Vibration* (Academic Press, New York NY, 1986).

12 T.F. Brooks and T.H. Hodgson, "Trailing edge noise prediction from measured surface pressures," J. Sound Vibr., **78**(1), 69-117 (1981).

13 F.V. Hutcheson and T.F. Brooks, "Measurement of trailing edge noise using directional array and coherent power methods," 8th AIAA/CEAS Aeroacoustics Conference, AIAA Paper 2002-2472 (2002).

14 J.C. Hutchenson and T.F. Brooks, "Effects of angle of attack and velocity on trailing edge noise,' 42nd AIAA Aerospace Science Meeting, AIAA Paper 2004-1031 (2004).

15 P. Migliore and S. Oerlemans, "Wind tunnel aeroacoustic tests of six airfoils for use on small wind turbines," NREL CP-500-3500 (2003).

16 S. Oerlemanns and P. Migliore, "Aeroacoustic wind tunnel tests of wind turbine airfoils," 10th AIAA/CEAS Aeroacoustics Conference, AIAA Paper 2004-3042 (2004).

17 S. Moreau and M. Roger, "Competing broadband noise mechanisms in low speed axial fans," 10th AIAA/CEAS Aeroacoustics Conference, AIAA Paper 2004-3039 (2004), accepted for publication in AIAA J., (2005).

18 R.W. Paterson and R.K Amiet, "Noise of a model helicopter rotor due to ingestion of turbulence," NASA CR 3213 (1979).

19 S. Moreau, M. Roger and V. Jurdic, "Effect of angle of attack and airfoil shape on turbulence-interaction noise," 11th AIAA/CEAS Aeroacoustics Conference, AIAA Paper 2005-2973 (2005).

20 S. Moreau, M. Henner, G. Iaccarino, M. Wang and M. Roger, "Analysis of flow conditions in freejet experiments for studying airfoil self-noise," AIAA J., **41**(10), 1895-1905 (2003).

21 H. Arbey and J. Bataille, "Noise generated by airfoil profiles placed in a uniform laminar flow," J. Fluid Mech., **134**, 33-47 (1983).

22 M. Roger and S. Moreau, "Broadband self-noise from loaded fan blades," AIAA J., **42**(3), 536-544 (2004).

23 M.S. Howe, "Edge-source acoustic Green's function for an airfoil of arbitrary chord with application to trailing-edge noise," The Quarterly J. of Mechanics and Applied Math., **54**(1), 139-155 (2001).

24 A. Oberai, F. Roknaldin and T.J.R. Hughes, "Computation of trailing edge noise due to turbulent flow over an airfoil," AIAA J., **40**(11), 2206-2216 (2002).

25 R. Schlinker and R.K. Amiet, "Helicopter trailing edge noise," NASA CR-3470 (1981).

26 J.C. Yu and M.C. Joshi, "On sound radiation from the trailing edge of an isolated airfoil in a uniform flow," AIAA Paper 79-0603 (1979).

27 S. Moreau and M. Roger, "Effect of airfoil aerodynamic loading on trailing-edge noise sources," AIAA J., **43**(1), 41-52 (2005).

28 J.M.R. Graham, "Similarity rules for thin aerofoils in non-stationary subsonic flows," J. Fluid Mech., **43**(4), 753-766 (1970).